

The effect of magnetospheric refraction on the morphology of pulsar profiles

S.A. Petrova

Institute of Radio Astronomy, Chervonopraporna St.4, Kharkov, 61002 Ukraine (rai@ira.kharkov.ua)

Received 7 March 2000 / Accepted 19 May 2000

Abstract. Refraction of ordinary superluminal waves in an ultrarelativistic highly magnetized plasma of pulsars is considered. The effect is found to cause an essential redistribution of rays in final directions which leads to the formation of separate components in pulse profiles. It is shown that refraction of waves in pulsar magnetospheres can account for the main features of profile morphology given that the hollow-cone emission model is the case. The observed frequency evolution of pulsar profiles appears to be well explained by the frequency dependence of the refraction efficiency if one also takes into account the effects of observational geometry. Special attention is paid to the interpretation of the inner conal components within the frame of our model.

Key words: plasmas – waves – stars: pulsars: general

1. Introduction

Pulsar magnetospheres are known to be filled with an ultrarelativistic highly magnetized electron-positron plasma. It streams along the open field lines of a dipolar magnetic field and ultimately leaves the magnetosphere. Undoubtedly, it is the plasma of the open field line tube that gives rise to pulsar radio emission, though the emission mechanism itself is still uncertain. Narrowness and stability of the observed pulses imply that radio emission originates well within the magnetosphere. So wave propagation should be influenced by the ambient plasma.

At pulsar conditions refraction of radio waves was found to be significant (Barnard & Arons 1986; Lyubarskii & Petrova 1998). Deviation of rays appears to be chiefly determined by the plasma density gradient across the open field line tube. The waves are believed to originate at frequencies of the order of the local Lorentz-shifted proper plasma frequency,

$$\omega \sim \omega_p \sqrt{\gamma}, \quad (1)$$

where γ is the plasma Lorentz-factor, ω_p the customary plasma frequency. The point is that the waves excited by the plasma instability should suffer intense induced scattering off the plasma particles, whereupon they acquire the frequencies (1) (Lyubarskii 1996). The plasma flow widens with the distance from the neutron star due to open field line tube widening. There-

fore radius-to-frequency mapping is the case: the lower the frequency of the wave the higher its origin lies. On the other hand, widening of the plasma flow entails decrease of transverse density gradient and, consequently, deviation of the rays originating at large distances is considerably diminished. Thus refraction turns out to be frequency-dependent, being the most prominent at high frequencies.

The observed pulse width can be substantially influenced by this effect. Pulse width versus frequency curves obtained with account for refraction are in qualitative agreement with the observed ones (Lyubarskii & Petrova 1998). In particular, the so-called “absorption feature” on the frequency dependence of pulse width observed in some pulsars (e.g., Rankin 1983b) can be explained in terms of refraction.

Further investigation shows that refraction can also determine the formation of separate components in pulsar profiles (Petrova & Lyubarskii 2000). According to standard models (e.g., Arons & Scharlemann 1979), beyond the edge of the open field line tube as well as near the magnetic axis the plasma number density is negligible. One can expect that it decreases towards both the magnetic axis and tube edges. So the open field line tube is thought to contain two regions (the inner and outer ones) with oppositely directed transverse gradient of the plasma density. Obviously, as a result of refraction rays deviate in the direction of plasma density decrease. Hence, the rays emitted in the inner part of the open field line tube deviate towards the magnetic axis and can be recognized as core emission, whereas those emitted in the outer tube part deviate away from the axis and form conal satellites. Note that the rays deviating towards the magnetic axis can intersect it, so that the core component has the maximum in the profile centre, though radio emission is believed to originate within the hollow cone, since the emission process is associated with the plasma.

At high frequencies the separation of profile components becomes increasingly prominent because of more efficient refraction. Such frequency evolution is consistent with that observed for triple profiles (Rankin 1983a). It should be noticed that the difference in polarization characteristics of the core and conal components (Rankin 1983a) can also be interpreted in terms of propagation effects in the magnetospheric plasma, namely, in terms of polarization-limiting effect (Petrova & Lyubarskii 2000). Thus the formation and physical properties of triple pro-

file components can be explained within the frame of primordial hollow-cone emission model taking into account propagation effects in pulsar plasma.

In the present paper we extend these ideas toward multiple profiles. The five-component profiles having an additional pair of conal satellites around the core component are known to represent a basic type of multiple profiles (Rankin 1983a, 1990, 1993; Gil, Kijak & Sieradakis 1993). In the spirit of the above ideas we suggest an interpretation of the origin of the inner emission cone. For this purpose we take into consideration the rays suffering particularly strong refraction in the inner part of the open field line tube. In this case the magnetic axis is intersected not only by the wave vector but also by the ray trajectory, so that the ray arrives into another half of the tube, where the wave vector turns round and starts deviating in the opposite direction (again towards the axis) due to transverse density gradient. It will be demonstrated that such rays can indeed account for the inner conal components of pulsar profiles.

The spectral properties of the inner-cone emission can also be attributed to the frequency dependence of refraction. At lower frequencies refraction becomes less efficient, so that the inner cone ultimately disappears and the multiple profile turns into the triple one. This is just what is observed (e.g., Rankin 1983a). At high frequencies the inner cone diverges with the frequency due to increasingly strong refraction. This divergence competes with the tube shrinkage, so that the resulting separation of the inner conal components can either increase with the frequency or decrease not so rapidly as in the case of outer conal components. Such trends also agree with the observations (Suleymanova & Pugachev 1998; Wu et al. 1998). Thus the multiple profiles can also be explained in terms of refraction of the hollow-cone emission.

So the present paper continues a detailed investigation of the impact of refraction in pulsar plasma on the observed pulsar radiation pattern. In particular, we concentrate on the formation and frequency evolution of multiple pulsar profiles. Sect. 2 contains general equations describing refraction of rays in pulsar plasma. The main features of ray propagation are outlined there as well. In Sect. 3 we study the formation of pulsar profiles with account for refraction. In Sect. 4 the frequency evolution of the simulated profiles is compared with the observationally established trends. Special attention is paid to the origin and properties of the inner conal components. The results are summarized in Sect. 5.

2. General theory of refraction in pulsar plasma

2.1. Ray equations

Refraction of waves in pulsar plasma was first considered by Barnard & Arons (1986). At pulsar conditions the effect was found to be essential for the low-frequency subluminal waves. However, direct escape of these waves from the magnetospheric plasma is impossible because of Landau damping. The wave transition to the superluminal branch of the dispersion curve in the course of linear coupling does not occur in this case (Bliokh & Lyubarskii 1996). Though, the subluminal waves can be

converted into the superluminal ones as a result of induced scattering off the plasma particles and subsequently escape from the magnetosphere. This process appears to be rather intensive in pulsar plasma (Lyubarskii 1996). Then we come to the problem on refraction of the superluminal waves ‘originating’ at the frequencies $\sim \omega_p \sqrt{\gamma}$. In this case refraction is weaker, however, it can be essentially enhanced if the plasma density gradient across the open field line tube is taken into account. This possibility was first pointed out by Barnard & Arons (1986). Our final equations include the transverse density gradient and therefore are somewhat different from the results of that paper, so we shall go through the model once more.

Let us consider a highly magnetized ultrarelativistic electron-positron plasma which is cold in the proper rest frame. This plasma is known to allow three normal wave modes. One of them, namely extraordinary wave, has the vacuum dispersion law and therefore propagates without suffering refraction. The dispersion relation describing two ordinary wave modes is given by (see, e.g., review by Lyubarskii 1995):

$$\left(1 - n_{\parallel}^2\right) \left(1 - \frac{\omega_p^2}{\omega^2 \gamma^3 (1 - n_{\parallel} \beta)^2}\right) - n_{\perp}^2 = 0, \quad (2)$$

where β is the plasma velocity in units of c , $\beta \equiv \sqrt{1 - 1/\gamma^2}$, $n_{\parallel} = ck_{\parallel}/\omega$, $n_{\perp} = ck_{\perp}/\omega$, with k_{\parallel} , k_{\perp} being the wave vector components parallel and perpendicular to the magnetic field direction, respectively,

$$\omega_p = \sqrt{\frac{4\pi N e^2}{m}},$$

N is the plasma number density, m the electron mass. As discussed above, of the two ordinary wave modes we are interested only in the superluminal one.

Since all the scale lengths in pulsar magnetosphere substantially exceed the wavelengths of radio emission, wave propagation in pulsar plasma can be treated in terms of geometrical optics. Given the dispersion relation (2), Hamilton’s equations can be written as (Barnard & Arons 1986):

$$\begin{aligned} \frac{1}{c} \frac{d\mathbf{x}}{dt} &= p\mathbf{n} - q\mathbf{b}, \\ \frac{1}{\omega} \frac{d\mathbf{k}}{dt} &= q \frac{\partial \mathbf{b}}{\partial \mathbf{x}} \cdot \mathbf{n} - l \frac{\partial \ln N}{\partial \mathbf{x}}, \end{aligned} \quad (3)$$

where \mathbf{n} and \mathbf{b} are the unit vectors along the wave vector and magnetic field, respectively,

$$\begin{aligned} p &= (1 + \eta)^3/d, \quad q = 4(1 - \eta)/(f^2 d), \\ l &= 2(1 + \eta)(1 - n_{\parallel}^2)/(f^2 d), \\ \eta &= 2\gamma^2(1 - n_{\parallel}), \\ d &= (1 + \eta)^3 - 4(1 - \eta)(1 - \eta/(2\gamma^2))/f^2, \\ f &= \frac{\omega}{\omega_p \sqrt{\gamma}}. \end{aligned} \quad (4)$$

The magnetic field is supposed to be dipolar. Let us choose the polar coordinate system with the axis along the magnetic axis. Then at a point with the polar coordinates (r, χ) the vector

b makes the angle $3\chi/2$ to the axis. Provided that the ray is emitted along the magnetic field line, the angle θ between the wave vector and magnetic axis is expected to remain of order χ all over the ray trajectory. Both these quantities are considered to be small, since the open field line tube is narrow. Then Eq. (3) can be rewritten as:

$$\begin{aligned} \frac{1}{c} \frac{dr}{dt} &= pn_{\parallel} - q, \\ \frac{r}{c} \frac{d\chi}{dt} &= pn_{\parallel}(\theta - \chi) - \frac{\chi q}{2}, \\ \frac{1}{c} \frac{dn_{\parallel}}{dt} &= -l \frac{\partial \ln N}{\partial r} + \frac{l\chi}{r} \frac{\partial \ln N}{\partial \chi}, \\ \frac{n_{\parallel}}{c} \frac{d\theta}{dt} &= \frac{3qn_{\parallel}}{2r} \left[\theta - \frac{3}{2}\chi \right] \\ &\quad - \frac{l}{r} \frac{\partial \ln N}{\partial \chi} - l \frac{\partial \ln N}{\partial r} [\chi - \theta]. \end{aligned} \quad (5)$$

The set of equations can be somewhat simplified. Dividing the equations of the set by the first one in order to eliminate time dependency and replacing one of the equations by the dispersion relation (2) we obtain:

$$\begin{aligned} r \frac{d\chi}{dr} &= \frac{1}{pn_{\parallel} - q} \left[pn_{\parallel} \left(\frac{3}{2}\theta - \chi \right) - \frac{\chi q}{2} \right], \\ n_{\parallel} \frac{d\theta}{dr} &= \frac{1}{pn_{\parallel} - q} \left[\frac{3qn_{\parallel}}{2r} (\theta - \chi) - \frac{2l}{3r\chi_0^2} \frac{\partial \ln N}{\partial \chi} \right. \\ &\quad \left. - l \frac{\partial \ln N}{\partial r} \left(\frac{2}{3}\chi - \theta \right) \right], \\ \eta \left(1 - \frac{4N}{f_0^2 r^3 (1 + \eta)^2} \right) & \\ - \frac{9}{4} \chi_0^2 \gamma^2 (\theta - \chi)^2 &= 0. \end{aligned} \quad (6)$$

Here the quantities r , χ , θ and N are normalized by their initial values and it is taken into account that $\theta_0 = 3\chi_0/2$; the subscript "0" refers to the initial values.

2.2. Plasma density distribution

To proceed further we are to specify the concrete plasma density distribution. Continuity of the plasma flow within the open field line tube implies that along a fixed field line the density decreases with the distance from the neutron star as r^{-3} , whereas the law of density distribution across the tube is uncertain. According to standard models, the plasma of the open field line tube is produced as a result of conversion of curvature gamma photons emitted by the primary particles streaming along the open field lines. Near the axis magnetic lines are nearly straight, so that the plasma density in this region is expected to be negligible. Keeping in mind the above considerations we choose the following distribution of the plasma density:

$$N = \begin{cases} N_0 \left(\frac{r_0}{r} \right)^3 \exp \left(-\varepsilon_1 \frac{(\chi - \chi_c \sqrt{r/r_0})^2}{(\chi_c \sqrt{r/r_0})^2} \right), & |\chi| \leq \chi_c \sqrt{r/r_0} \\ N_0 \left(\frac{r_0}{r} \right)^3 \exp \left(-\varepsilon_2 \frac{(\chi - \chi_c \sqrt{r/r_0})^2}{(\chi_c \sqrt{r/r_0})^2} \right), & |\chi| \geq \chi_c \sqrt{r/r_0}, \end{cases} \quad (7)$$

where ε_1 and ε_2 are the constants. Thus the density has the maximum value on the two characteristic field lines passing through the points (r_0, χ_c) and $(r_0, -\chi_c)$, correspondingly, and it monotonically decreases towards both the magnetic axis and tube edges.

Differentiation of Eq. (7) yields:

$$\begin{aligned} \frac{\partial \ln N}{\partial \chi} &= -2\varepsilon \frac{\chi - \chi_c \sqrt{r/r_0}}{(\chi_c \sqrt{r/r_0})^2}, \\ \frac{\partial \ln N}{\partial r} &= -\frac{3}{r} + \frac{\varepsilon}{\chi_c^2} \frac{(\chi - \chi_c \sqrt{r/r_0})(\chi + 3\chi_c \sqrt{r/r_0})}{r^2}, \end{aligned} \quad (8)$$

with

$$\varepsilon = \begin{cases} \varepsilon_1, & |\chi| \leq \chi_c \sqrt{r/r_0} \\ \varepsilon_2, & |\chi| \geq \chi_c \sqrt{r/r_0}. \end{cases}$$

Substituting Eq. (8) in Eq. (6) and recalling the definitions (4) we obtain finally:

$$\begin{aligned} r \frac{d\chi}{dr} &= \frac{\chi}{2} + \frac{3(1 + \eta)^3}{2A} (\theta - \chi), \\ \frac{d\theta}{dr} &= \frac{6(1 - \eta)N(\theta - \chi)}{Ar f_0^2} \\ &\quad + \frac{8\varepsilon(1 + \eta)\eta N [\chi\chi_0 / (\chi_c \sqrt{r}) - 1]}{3Ar^{3/2} f_0^2 \chi_0 \chi_c \gamma^2}, \\ \eta \left(1 - \frac{4N}{f_0^2 r^3 (1 + \eta)^2} \right) & \\ - \frac{9}{4} \chi_0^2 \gamma^2 (\theta - \chi)^2 &= 0, \end{aligned} \quad (9)$$

where

$$A \equiv (1 + \eta)^3 - \frac{4(1 - \eta)N}{f_0^2}$$

and the quantities r , χ , θ , N are also normalized by their initial values.

In the second equation of the set (9) the term corresponding to the radial density gradient is neglected, since it is of the order of γ^{-2} . The first addend in the right-hand side of this equation is of order unity, while the second one is of the order of $\varepsilon(\chi_0 \chi_c)^{-1} \gamma^{-2}$, which can be greater than unity given sufficiently small angles. So for the rays emitted closer to the magnetic axis (at smaller χ_0) and deeper in the magnetosphere (for a fixed characteristic field line smaller χ_c imply smaller r_0) refraction can be particularly efficient. Then it is determined by transverse gradient of the plasma density.

Note that the qualitative picture of plasma distribution across the open field line tube is of crucial importance, since the sign of transverse density gradient determines the direction of ray deviation. However, the concrete shape of density profile is inessential, because the value of wave vector deviation is determined by $\frac{\partial \ln N}{\partial \chi}$ (cf. Eq. (6)).

It should be pointed out that the wave frequency, ω , and plasma density at the emission origin, N_0 , enter Eq. (9) only as a combination $\frac{\omega}{\omega_{p0}\sqrt{\gamma}} \equiv f_0$. Hereafter we shall suppose that for all frequencies $f_0 = \text{const} \sim 1$, i.e. radius-to-frequency mapping is the case. Note that Eq. (9) does not contain the emission altitude, r_0 , explicitly. So the decrease of transverse density gradient with r_0 because of the tube widening ($\chi_c^{-1} \propto r_0^{-1/2}$) entirely determines the frequency dependence of refraction efficiency. Radius-to-frequency mapping implies that for a fixed characteristic field line $\omega \propto r_0^{-3/2} \propto \chi_c^{-3}$.

2.3. Characteristic features of refraction

The set of Eqs. (9) describes wave vector deviation and the trajectory of an ordinary wave in an ultrarelativistic highly magnetized plasma. Numerical solutions of the set obtained for various values of χ_c are shown in Fig. 1. For a fixed characteristic field line the lower values of χ_c imply the lower emission altitudes and, correspondingly, the higher frequencies. The rays considered are emitted in the inner part of the open field line tube, i.e. $\chi_0 < \chi_c$.

As can be seen in Fig. 1a, the wave vector deviates towards the magnetic axis and intersects it. The trajectory does not cross the axis, though also bends toward it. At lower emission altitudes refraction becomes stronger and the trajectory crosses the axis (Fig. 1b). Since beyond the axis transverse density gradient has the opposite sign, the wave vector starts deviation in the opposite direction, i.e. again toward the axis. If refraction is still stronger, \mathbf{k} can intersect the axis once more (Fig. 1c). At the same time, the trajectory repeatedly starts bending towards the axis.

The behaviour of the rays emitted in the outer part of the open field line tube is more trivial. Both θ and χ increase monotonically, the final enhancement being larger at lower emission altitudes (see also Lyubarskii & Petrova 1998).

3. Pulse profiles with account for refraction

3.1. Ray grouping

Now let us consider how refraction of rays in pulsar plasma influences the formation of the observed pulse profile. Note that our investigation is concerned only with the “proper” pulsar profiles, i.e. with the profiles not distorted by observational geometry. These profiles are really observed if the sight line traverses the emission cone along the diameter. In the case of noncentral cuts of the emission cone the profiles obtained can differ essentially in the number of components (e.g., Rankin 1983a) and in the spectral evolution (Sieber 1997). Since the effects of observational geometry are well-studied, we ignore them in our consideration and concentrate on the intrinsic characteristics of pulsar radiation pattern.

Within the frame of our simplified two-dimensional scheme, the pulse profile is constructed of the rays emitted at the same altitude, r_0 , and at all possible polar angles, χ_0 , inside the open field line tube (recall that the rays are emitted along the magnetic field lines, i.e. $\theta_0 = 3\chi_0/2$). To analyse the ultimate intensity

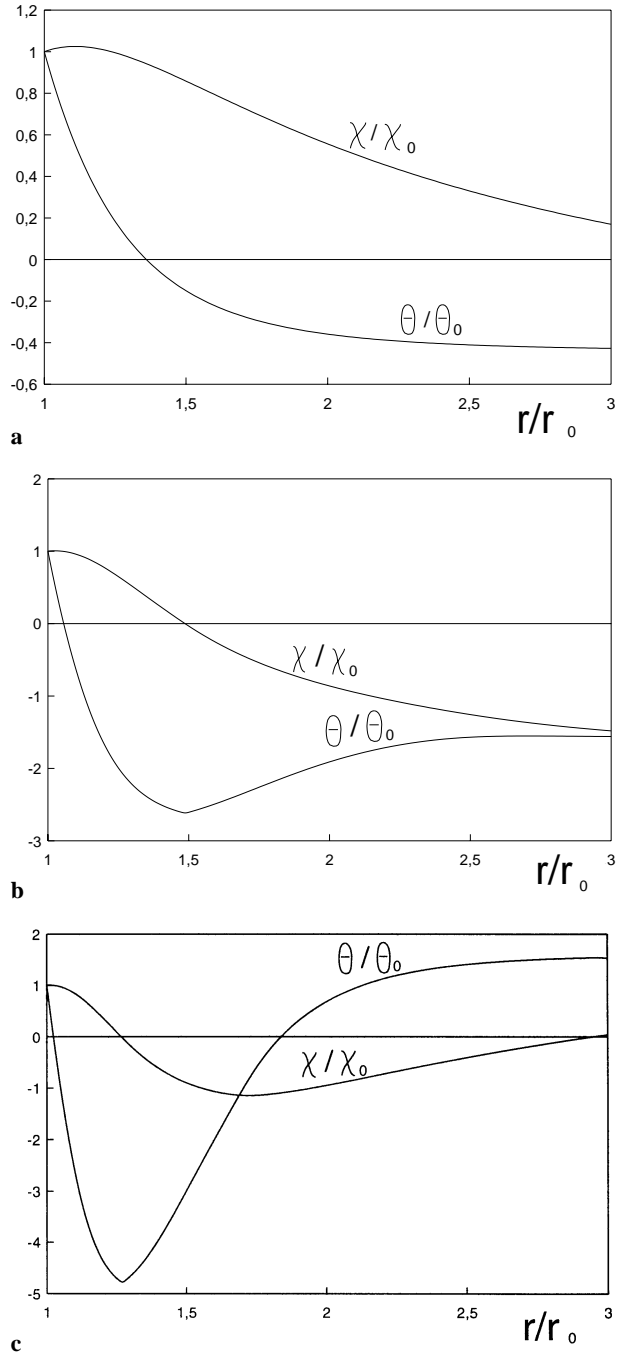


Fig. 1a–c. Ray trajectories and wave vector deviation vs. radius: **a** $\chi_c = 0.03$, **b** $\chi_c = 0.015$, **c** $\chi_c = 0.01$; $\gamma = 30$, $f_0 = 0.5$, $\varepsilon_1 = 3$, $\varepsilon_2 = 4$, $\chi_0 = 0.5\chi_c$

distribution within the profile we are to examine the phase trajectories of these rays in the space of the quantities r and θ with account for refraction. As shown in the previous section, the wave vector orientation can evolve considerably in the course of ray propagation in pulsar plasma (see Fig. 1). The final values of θ versus the initial ones are plotted in Fig. 2. The dependences are calculated on the basis of Eq. (9) for three various values of χ_c (i.e. for various emission altitudes r_0 and, correspondingly,

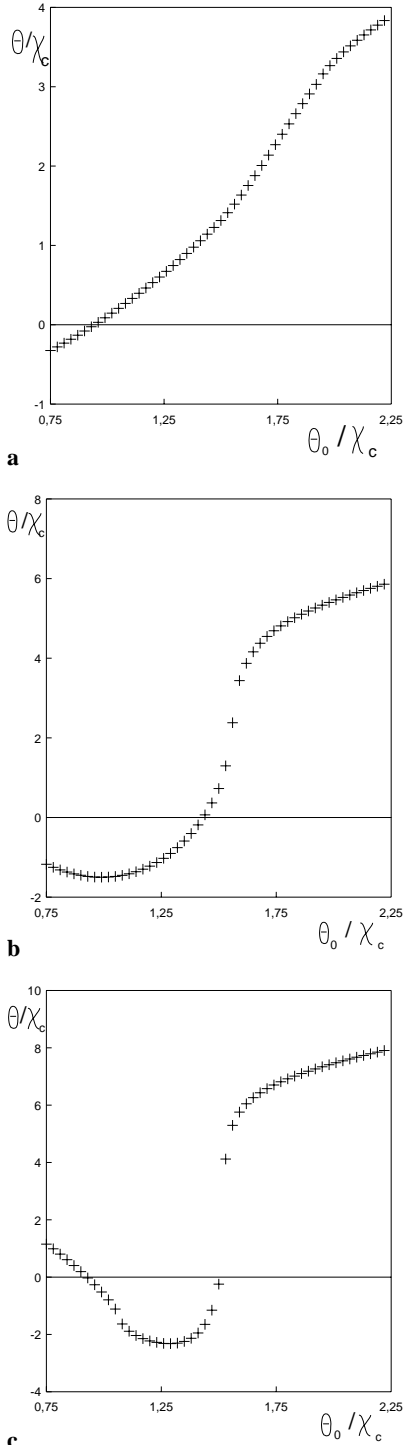


Fig. 2a–c. Final ray directions vs. initial ones; parameters are the same as in Fig. 1; $0.5\chi_c \leq \chi_0 \leq 1.5\chi_c$

for various frequencies). Due to the symmetry of the problem we consider only positive θ_0 . The abscissae of the points plotted are equidistant, so that visible nonuniformity in the distribution of the points along a curve corresponds to ray grouping in the course of refraction.

The rays emitted in the outer part of the open field line tube ($\theta_0 \equiv 3\chi_0/2 > 3\chi_c/2$) deviate away from the magnetic axis, so that the angle θ increases along the trajectory. According to the second equation of the set (9), the more the polar angle differs from χ_c — the greater the rate of ray deviation. On the other hand, if the ray deviates too intensely, the trajectory severely bends toward the tube edge and very soon comes into the region poor in the plasma, so that refraction ceases. Therefore one can observe ray grouping toward the highest final θ , the effect becoming more prominent at higher frequencies (see Fig. 2).

The rays emitted in the inner part of the open field line tube deviate toward the magnetic axis and can intersect it. Given that refraction is particularly strong, the rays have time to start deviation in the opposite direction, since their trajectories also cross the magnetic axis. Take note of the concentration of rays near the turning-point (Fig. 2b,c). It should be also pointed out that at higher frequencies the turning-point moves away from the magnetic axis.

3.2. Frequency evolution of pulse profile

Apparently, ray grouping because of refraction testifies to an essential intensity redistribution within the pulsar profile. The final profiles themselves can be obtained as follows. Energy conservation along the phase trajectories of rays implies that

$$dW = W_{\theta_0}(r_0, \theta_0)d\theta_0 = W_{\theta}(r, \theta)d\theta, \quad (10)$$

where W is the total radiated power, $W_{\theta_0}(r_0, \theta_0)$ and $W_{\theta}(r, \theta)$ are the angular distributions of the power at the emission origin and at the distance r , respectively. Using Eq. (9) in Eq. (10) one can trace the evolution of radiation pattern on account of refraction.

Let us first assume that the rays are emitted within the hollow cone, with the intensity being uniform:

$$W_{\theta_0}(r_0, \theta_0) = \begin{cases} 1, & \frac{3}{4}\chi_c \leq |\theta_0| \leq \frac{9}{4}\chi_c, \\ 0, & |\theta_0| < \frac{3}{4}\chi_c \text{ and } |\theta_0| > \frac{9}{4}\chi_c. \end{cases} \quad (11)$$

Of course, uniform intensity distribution is hardly a good approximation for real pulsars. However, using this distribution allows to illustrate evidently the main features of profile formation due to refraction. The initial intensity distribution of a more realistic form will be considered in the next subsection.

The profiles obtained through numerical solution of Eqs. (9)–(10) together with Eq. (11) are shown in Fig. 3. They are calculated for the set of χ_c , that is for the set of frequencies related to each other as 1 : 1.6 : 2.7 : 5.3 : 12.7 : 24.8. As mentioned above, we consider the profiles resulting from the central cut of the radiation beam by the sight line, so that the pulse longitude, ϕ , is equivalent to the angle θ the ray makes finally with the magnetic axis. One can see that moderate refraction (at sufficiently low frequencies) can cause the triplicity of pulsar profiles. The rays emitted in the inner part of the open field line tube become finally almost aligned with the magnetic axis giving rise to the core component of the profile. The conal satellites are constructed of the rays originating in the outer part of the tube; their final directions tend to group at the periphery

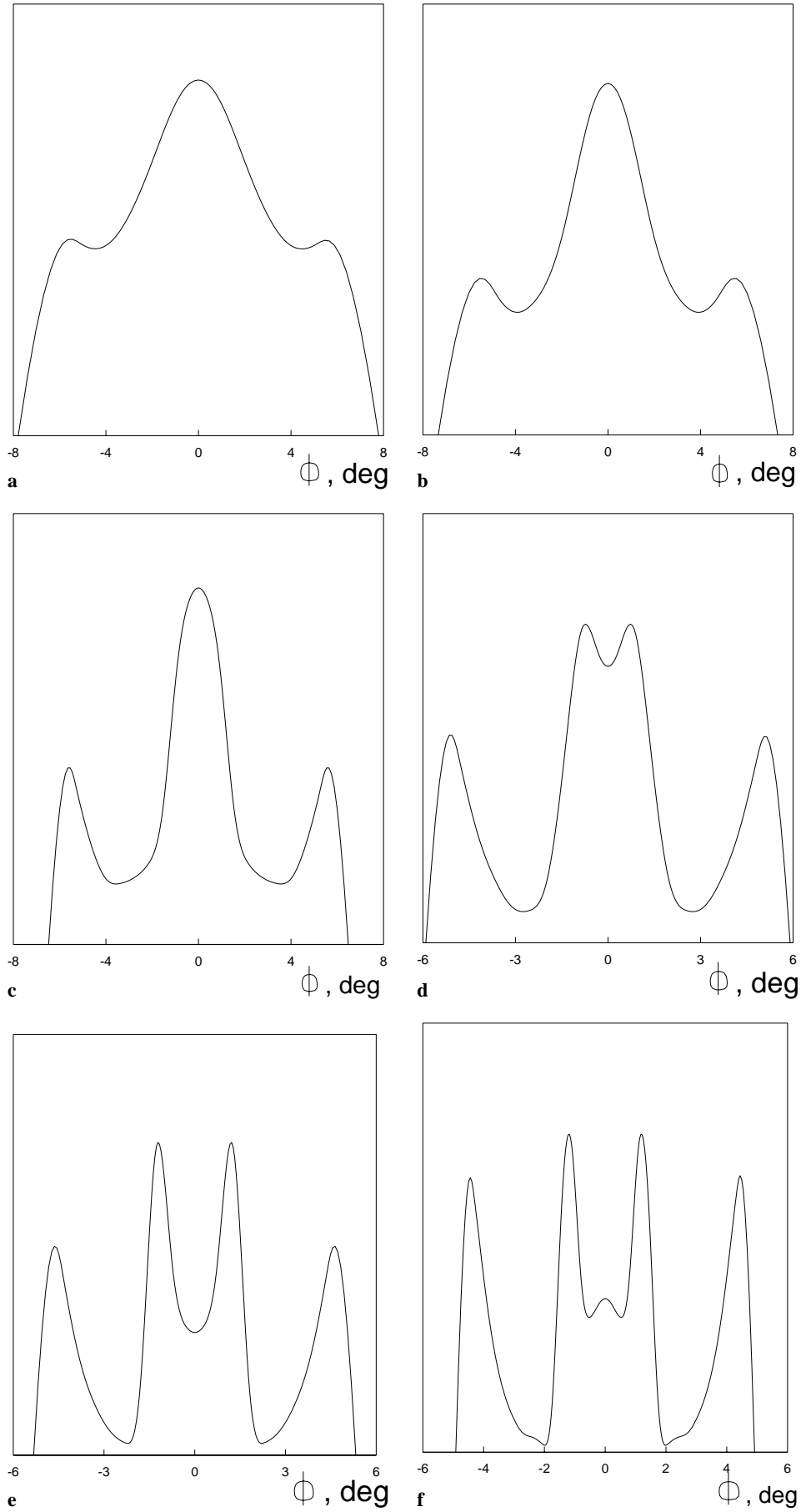


Fig. 3a–f. Pulse profiles with account for refraction: **a** $\chi_c = 0.035$, **b** $\chi_c = 0.03$, **c** $\chi_c = 0.025$, **d** $\chi_c = 0.02$, **e** $\chi_c = 0.015$, **f** $\chi_c = 0.012$; the rest parameters are the same as in Figs. 1 and 2

of the profile. The separation of profile components increases with the frequency (see Fig. 3a-c).

At still higher frequencies one can observe the splitting of the central component into two gradually diverging halves (Fig. 3d-e). These inner components consist of the rays whose trajectories intersect the magnetic axis and come into the opposite half of the open field line tube, whereupon the wave vector turns round and starts deviation in the opposite direction (cf. Fig. 1b). As is evident from Fig. 2b, the turning-point corresponds to the longitude of intensity maximum. Note that each inner component is formed by the rays originating in the opposite half of the tube (negative final θ correspond to positive θ_0 and vice versa). If refraction is extremely strong, the rays emitted sufficiently close to the magnetic axis can give rise to an additional component in the profile centre (Fig. 3f). In this case the wave vectors have time to intersect the magnetic axis once more (cf. Fig. 1c, 2c). Note that the core of the five-component profile may arise in an alternative way (see below).

The values of χ_c in Figs. 3a-f can be related to the frequencies of radio emission. First of all, it is convenient to normalize the plasma number density at the surface of the neutron star by the Goldreich-Julian charge density:

$$N_\star = \frac{\kappa B_\star}{ceP},$$

where κ is the plasma multiplicity factor, B_\star the magnetic field strength at the stellar surface, P the pulsar period. Then we find:

$$N_0 = 6.25 \cdot 10^{13} P^{-1} \kappa_3 B_{\star 12} \left(\frac{r_\star}{r_0} \right)^3 \text{ cm}^{-3},$$

with r_\star being the stellar radius, $\kappa_3 \equiv \frac{\kappa}{10^3}$, $B_{\star 12} \equiv \frac{B_\star}{10^{12} \text{ G}}$. In addition, location of the characteristic field line within the open field line tube should be specified, i.e. the ratio $\xi \equiv \frac{\chi_c}{\chi_t}$ should be given, where χ_t is the polar angle of the boundary open field line, $\chi_t = \sqrt{r_0/r_L}$, r_L is the light cylinder radius, $r_L = 5 \cdot 10^9$ cm. Then keeping in mind that $2\pi\nu = f_0 \omega_{p0} \sqrt{\gamma}$ one can express the observed frequency:

$$\nu = 2f_0 P^{-2} (\kappa_3 \gamma_2 B_{\star 12})^{1/2} r_{\star 6}^{3/2} \xi^3 \chi_c^{-3} \text{ MHz};$$

here $\gamma_2 \equiv \frac{\gamma}{10^2}$, $r_{\star 6} \equiv \frac{r_\star}{10^6 \text{ cm}}$. It should be noted that in theoretical models the value of the multiplicity factor varies within some orders of magnitude, $\kappa \sim 10^2 - 10^5$ (e.g., Arons & Scharlemann 1979; Arons 1983). Moreover, the location of the characteristic field line is uncertain. The values of f_0 and γ are also model-dependent. So the frequencies corresponding to Figs. 3a-f cannot be derived definitely. Note that the diversity in the pulse profile shapes observed for various pulsars at a fixed frequency testifies to a certain diversity of physical conditions in pulsar plasma. Unfortunately, the presence of a number of poorly known parameters does not allow to draw any definite conclusion about the physical characteristics of the pulsar plasma on the basis of the observed pulse profile. Here and hereafter we consider only the trends in the frequency evolution of the profiles obtained for the appropriate sets of parameters.

3.3. The effect of initial intensity distribution

Let us turn to a more realistic intensity distribution of the radiation emitted:

$$W_{\theta_0} = \begin{cases} \exp \left[-\alpha \varepsilon \frac{(2\theta_0/3 - \chi_c)^2}{\chi_c^2} \right], & \frac{3}{4}\chi_c \leq |\theta_0| \leq \frac{9}{4}\chi_c, \\ 0, & |\theta_0| < \frac{3}{4}\chi_c \text{ and } |\theta_0| > \frac{9}{4}\chi_c, \end{cases} \quad (12)$$

where α is the constant. Now $W_{\theta_0}(r_0, \theta_0)$ is described by the two Gaussians which peak at the characteristic field lines. Within the frame of the hollow-cone emission model this seems to be a reasonable approximation. The assumption that the original components in the emitted radiation pattern of pulsars can be represented by Gaussian shape is based first of all on statistical arguments and supported by the observed Gaussian shape of subpulses (e.g., Wu & Manchester 1992). Narrowness of subpulses implies that refraction has a minimum effect on their final shape, since all the rays constructing the subpulse evolve almost alike. Thus it is sensible to attribute the Gaussian shape to the original components of pulsar radiation pattern. Note that the observed pulse profiles are usually represented as a sum of Gaussians (e.g. Kramer et al. 1994). It should be kept in mind that taking into account refraction of radio waves in the magnetosphere implies that these Gaussians do not correspond to the physical components of pulsar emission. Nevertheless, the method of multicomponent Gaussian fits remains a useful tool for analysing the main features of profile composition and for tracing general trends of the spectral evolution.

The final profile shape appears to be essentially dependent on the angular distribution of intensity emitted, since different rays are influenced by refraction in different ways. The pulse profiles obtained for a set of $W_{\theta_0}(r_0, \theta_0)$ with account for refraction are presented in Fig. 4. Fig. 4a illustrates the case of the uniform intensity distribution (Eq. (11)), whereas Figs. 4b-c correspond to $W_{\theta_0}(r_0, \theta_0)$ described by Eq. (12) at various α . The rest parameters are identical. As can be seen in Fig. 4, the intensity near the pulse centre increases and, accordingly, both inner components weaken provided that the intensity emitted decreases toward the magnetic axis. The emission bridge at the profile centre turns into a separate component. The point is that the rays emitted close to the characteristic field line and suffering relatively weak refraction are now more numerous than those emitted at small polar angles and grouping near the turning-point due to strong refraction. So the quadruple profile can be transformed into the five-component one, if the proper distribution of intensity emitted is adopted.

Fig. 5 shows the spectral evolution toward lower frequencies for the profile plotted in Fig. 4c. One can see that the inner components merge, the profile becoming triple (Fig. 5a). At still lower frequencies the profile turns into a double one with the bridge of emission at the centre (Fig. 5b).

4. Discussion

The structure of pulsar profiles and their frequency evolution simulated in the previous section are confirmed by observations. The triple profiles appear to rank among the prevalent

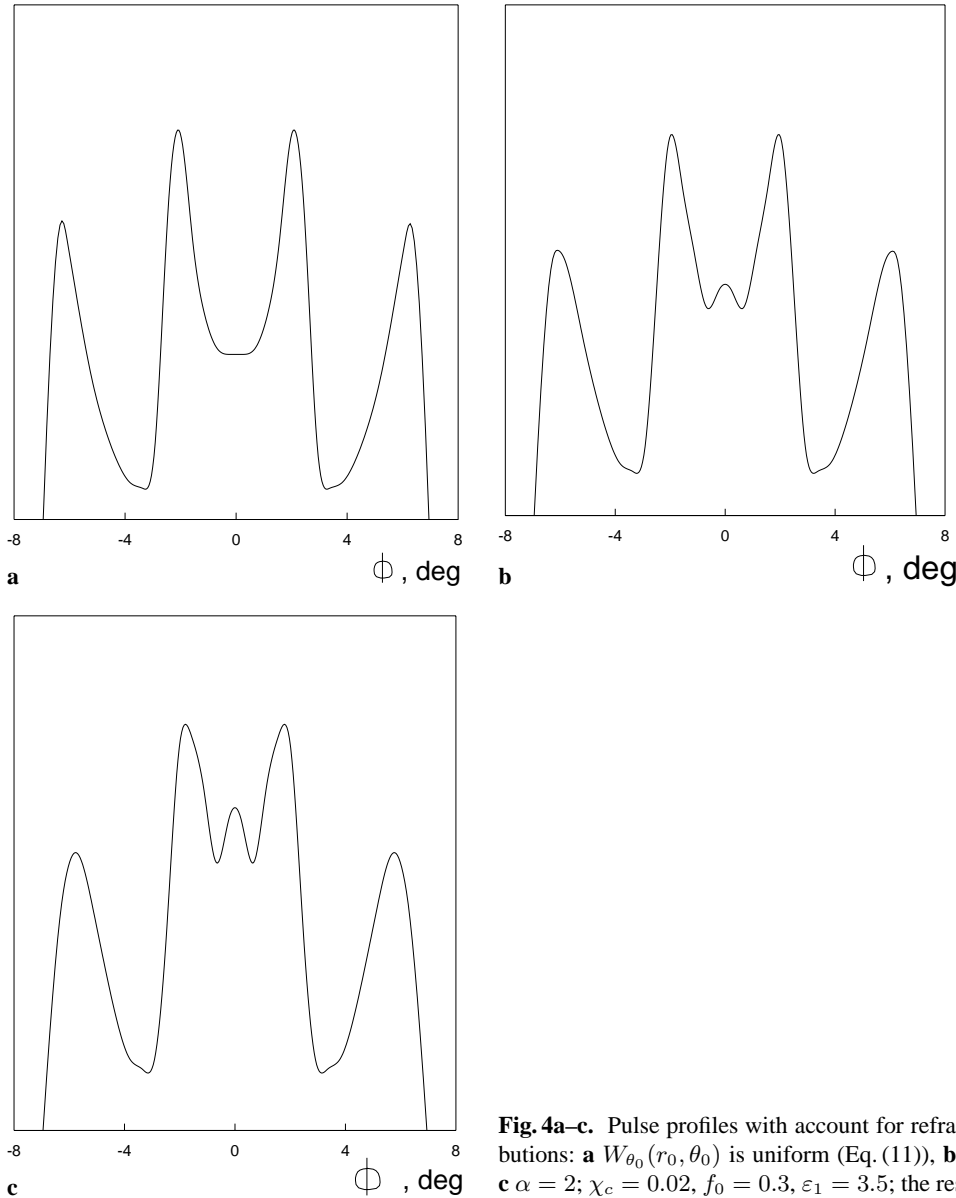


Fig. 4a–c. Pulse profiles with account for refraction given different initial intensity distributions: **a** $W_{\theta_0}(r_0, \theta_0)$ is uniform (Eq. (11)), **b** $W_{\theta_0}(r_0, \theta_0)$ is given by Eq. (12), $\alpha = 1$, $\alpha = 2$; $\chi_c = 0.02$, $f_0 = 0.3$, $\varepsilon_1 = 3.5$; the rest parameters are the same as in Fig. 3

pulsar profiles. As a rule the core component has a steeper spectrum compared with the conal satellites, so that the latter develop progressively with the frequency (Rankin 1983a). However, this does not necessarily mean that the core and conal components correspond to different emission mechanisms. As demonstrated by Sieber (1997), such spectral behaviour can be interpreted as a consequence of observational geometry. For a given pulsar the sight line traverses the emission beam at a proper distance from the centre, whereas the beam itself shrinks with the frequency because of radius-to-frequency mapping. As a result, the higher the frequency the smaller part of the core component remains visible, so that the core emission seems to become relatively weaker. The peculiar polarization properties of the core component, such as a high circular polarization and disorderly variation of the position angle of linear polarization (Rankin 1983a) can be attributed to the propagation effects in the magnetosphere, namely to the polarization-limiting effect (Petrova & Lyubarskii

2000). So the observed difference in both the spectral and polarization properties of the core and conal emission is not intrinsic to the emission mechanism itself. The investigation carried out in the previous section provides a physical ground for the explanation of the origin of the separated profile components given that radiation is emitted into a hollow cone.

According to Fig. 3, at sufficiently high frequencies the core component tends to split. Although this is not revealed as a basic trend of profile evolution and quadruple profiles are in general rare, several observations support the high-frequency core splitting. For instance, it can be seen in the profile of PSR 1946+35 at $\nu = 2650$ MHz (Lyne & Manchester 1988) and at $\nu = 4750$ MHz it becomes more prominent (Sieradakis et al. 1995), while at the lower frequency, $\nu = 1692$ MHz, the profile is the ordinary triple one (Lyne & Manchester 1988). The triple profile of PSR 1913+16 ($\nu = 430$ MHz) becomes quadruple at the higher frequency, $\nu = 1410$ MHz, on account of core splitting (Lyne

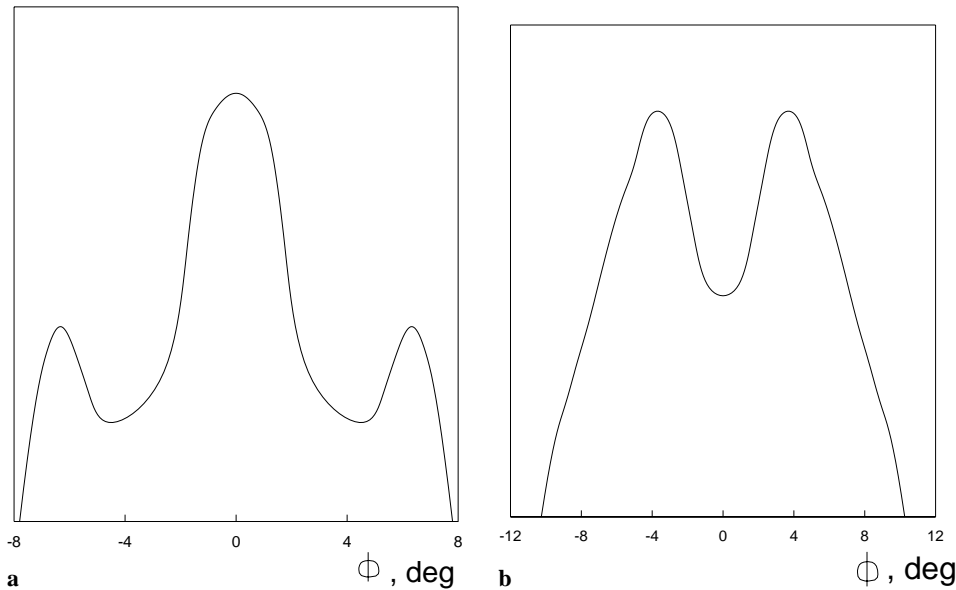


Fig. 5a and b. Profile evolution toward lower frequencies given the initial intensity distribution (12), **a** $\chi_c = 0.03$, **b** $\chi_c = 0.05$; the rest parameters are the same as in Fig. 4c

& Manchester 1988). Similarly, the profiles of PSR 0450-18 and PSR 1826-17 observed as triple at $\nu = 1420$ MHz (Lyne & Manchester 1988) and $\nu = 1400$ MHz (Sieradakis et al. 1995), respectively, are quadruple at $\nu = 5000$ MHz (Hoensbroech 1999) and $\nu = 4750$ MHz (Sieradakis et al. 1995), respectively.

Core splitting is also observed in the profiles with the so-called partial emission cones (e.g., PSR 0450+55 and PSR 0559-05 (Hoensbroech 1999)). These profiles are thought to be triple, with one of the conal components being too weak to be detected. One of the apparent components is recognized as the core according to its spectral and polarization properties. Keeping in mind that the conal emission can be sufficiently weak one can interpret an unusual frequency evolution of the profile of PSR 0611+22. At low frequencies it is specified as the conal single (Lyne & Manchester 1988 — $\nu = 400$ MHz; Sieradakis et al. 1995 — $\nu = 1400$ MHz), whereas at the frequency $\nu = 5000$ MHz it is an obvious double profile (Hoensbroech 1999). Note that the shrinkage of the emission cone with the frequency implies that the conal components should approach each other and ultimately merge. In the case of PSR 0611+22 the frequency evolution is inverse, therefore one can suppose that the profile is the core single and at high frequencies suffers splitting.

Although the high-frequency shrinkage of the emission cone can make the profile components overlap and merge, generally the high-frequency profiles look even more complex (see, e.g., Hoensbroech 1999). This feature may be attributed to the increasing role of refraction. Among the complex profiles the five-component ones appear to be the most abundant (Rankin 1983a, Wu et al. 1992). As the frequency decreases, they evolve as to become ultimately triple (e.g., Rankin 1983a). This trend can also be seen in our Figs. 4b, 5a.

As found in the previous section, at high frequencies increasingly strong refraction moves the maxima of the inner conal components away from the profile centre, while the whole emission cone shrinks. This effect can account for an essential difference observed in the frequency evolution of the inner and

outer conal radii. In contrast to the outer conal radius, which evidently decreases with the frequency, the inner one either increases or decreases too slowly (Wu et al. 1992; Suleymanova & Pugachev 1998; Wu et al. 1998).

It is also interesting to compare the frequency dependence of the inner conal radius with the frequency evolution of the width of the core component. In the case of PSR 0329+54 at low frequencies the inner conal radius decreases with the frequency, while at high frequencies it increases, the turning frequency, ν_c , being ≈ 270 MHz. The frequency dependence of the core width exhibits the so-called “absorption feature”, i.e. the monotonic decrease with the frequency is disturbed by a trough, with the local minimum at the bottom of the trough corresponding to the frequency ν_c (Suleymanova & Pugachev 1998). Note that the “absorption feature” has been already explained in terms of refraction (Lyubarskii & Petrova 1998). This feature was shown to be peculiar to the components formed by the rays originating in the inner part of the open field line tube, where the plasma density decreases toward the magnetic axis. If refraction is so efficient that even the rays emitted far enough from the magnetic axis deviate toward it intensely, the width of the core component decreases significantly. At higher frequencies the rays begin to intersect the axis and form an opposite half of the core component. Since the deviation increases with the frequency, the core width also increases until the rays have enough time to turn and start deviation in the opposite direction. The coincidence of the characteristic frequency of the trough in the frequency dependence of the core width with the turning frequency for the inner conal radius implies that ν_c is the frequency at which refraction is significant for all the rays emitted in the inner part of the open field line tube.

Within the scope of our discussion the inner conal components have much more in common with the core component than with the outer conal ones. Both the core and inner conal components are constructed of the rays originating in the inner part of the open field line tube. All these rays can be regarded

as “core” though they group into separate components due to refraction. Note that the rays emitted at different altitudes (i.e. at different frequencies) along a fixed field line can belong to different components, so that the validity of the proper separation into the components (e.g. by means of Gaussian fits) seems to be questionable. This is well illustrated by the spectra of the profile components in PSR 1451-68 (Wu et al. 1998). The spectral curves for both the core and inner conal components appear to vary drastically from point to point, whereas their sum seems to be a smooth curve similar to that obtained for the outer conal components. So the core and inner conal components can be better described as a triple core splitted by refraction.

5. Conclusions

We have considered refraction of ordinary superluminal waves in an ultrarelativistic highly magnetized plasma. The results are applied to studying the wave propagation in the open field line tube of a pulsar. It is shown that the main features of the morphology of pulsar profiles can be attributed to refraction of rays in the magnetosphere. Proceeding from the hollow-cone emission model and taking into account the apparent association of radio emission with the magnetospheric plasma we suggest the “hollow field line tube”, with the plasma density decreasing toward both the magnetic axis and tube edges. Then the rays emitted in the inner part of the tube deviate toward the axis and form the core component in the pulse profile, while those emitted in the outer tube part deviate away from the axis and give rise to the outer conal satellites. The inner conal components observed in a number of pulsar profiles are shown to be constructed of the rays originating sufficiently close to the magnetic axis and suffering extremely strong refraction. The spectral evolution of the simulated profiles appears to be compatible with the observed trends given that the effects of observational geometry are taken into account. So it is found that the basic species of the observed pulsar profiles can be explained in terms of primordial hollow-cone emission model if one takes into consideration refraction of radio waves in the magnetospheric plasma.

In principle, the results of the present paper imply that proceeding from the observed profile shape one can conclude about the physical conditions in the pulsar plasma. However, this reverse problem on diagnostics of the magnetospheric plasma is essentially complicated by the presence of a number of parameters. Moreover, true distributions of the plasma density and radiation intensity are obscure. Keeping in mind all this in the present paper we restricted ourselves only with outlining general consequences of magnetospheric refraction for pulse profile formation; the qualitative features are illustrated numerically for appropriate parameters. A more rigorous treatment based on a certain model of pulsar plasma can somewhat alter our quantitative results, while the principal ideas are thought to be the same.

It should be noted that our investigation is almost independent of the concrete emission mechanism. The radius-to-frequency mapping is the only our assumption. The waves are supposed to originate at the frequencies $\omega \sim \omega_p \sqrt{\gamma}$ and, con-

sequently, $r \propto \nu^{-\xi}$ with $\xi = 2/3$. From the theoretical point of view, such frequencies are acquired by the waves as a result of induced scattering off the plasma particles, which is rather efficient at pulsar conditions (Lyubarskii 1996). In principle, the observational data examined by different methods also testify to radius-to-frequency mapping, though as a rule ξ appears to be somewhat less. It should be pointed out that the observational results can themselves be essentially affected by refraction.

Thorough analysis of the vast data on pulsar profiles led Rankin (1993) and Gil et al. (1993) to the conclusion that the inner and outer conal radii depend on pulsar period as $P^{-1/2}$. Within the frame of our considerations this can be regarded as an additional indication that the efficiency of refraction (and, correspondingly, the location of profile components) is determined by the location of the characteristic field line, i.e. by the value of $\chi_c \propto \sqrt{r_0/r_L} \propto P^{-1/2}$; here r_L is the light cylinder radius. The factors in the $P^{-1/2}$ -dependencies of the conal radii appear to vary with the frequency. In the case of the inner conal radius this variation is disorderly (cf. the above discussion on the frequency dependence of the inner conal radius), while the outer conal radius progressively decreases with the frequency, though this decrease is weaker than that expected from the $\nu^{-2/3}$ -law (e.g. Kramer et al. 1994). The latter feature can be directly attributed to the influence of refraction, since at higher frequencies the effect is stronger and causes an additional separation of the outer conal components. Thus the power index ξ derived from examining the observed opening angles of the outer emission cone should be underestimated.

The radius-to-frequency mapping found by means of multifrequency pulsar timing (Phillips 1992) is also expected to be somewhat uncertain, since the time of arrival should be affected by refraction delays in pulsar magnetosphere. Another independent method of deriving radius-to-frequency mapping lies in analysing the shifts in the position angle curves with respect to the pulse centre (Blaskiewicz et al. 1991). However, this method is based on the assumption of a proper emission mechanism, namely the curvature emission of the plasma particles, and it does not take into account propagation effects in the magnetosphere.

Strictly speaking, given the plasma density distribution (7) our assumption that $\omega \sim \omega_p \sqrt{\gamma}$ does not imply an ordinary radius-to-frequency mapping, since the waves of a proper frequency originate along an isodense rather than at a fixed altitude. So close enough to the magnetic axis and to the tube edges the rays are emitted deeper than those in the vicinity of the characteristic field line. However, it is clear that taking into account these considerations can only strengthen the effects examined in the present paper. Indeed, for the rays emitted far from the characteristic field line (i.e. at smaller altitudes) refraction should be still more efficient. So ray grouping can be more prominent, while the qualitative features of profile formation are believed to remain the same.

References

Arons J.J., 1983, ApJ 266, 215

- Arons J.J., Scharlemann E.T., 1979, *ApJ* 231, 854
Barnard J.J., Arons J., 1986, *ApJ* 302, 138
Blaskiewicz M., Cordes J.M., Wasserman I., 1991, *MNRAS* 370, 643
Bliokh K.Yu., Lyubarskii Yu.E., 1996, *Pis'ma v Astron. Zh.* 22, 539
[English translation: *Astron. Lett.* 22, 482 (1996)]
Gil J.A., Kijak J., Sieradakis J.H., 1993, *A&A* 272, 268
Hoensbroech A.G., 1999, PhD Thesis, Bonn: Max-Planck Institute for Radio Astronomy
Kramer M., Wielebinsky R., Jessner A., et al., 1994, *A&AS* 107, 515
Lyne A.G., Manchester R.N., 1988, *MNRAS* 234, 477
Lyubarskii Yu.E., 1995, *Astrophys. Space Phys. Rev.* 9/ 2, 1
Lyubarskii Yu.E., 1996, *A&A* 308, 809
Lyubarskii Yu.E., Petrova S.A., 1998, *A&A* 333, 181
Petrova S.A., Lyubarskii Yu.E., 2000, *A&A* 355, 1168
Phillips, 1992, *ApJ* 385, 282
Rankin J.M., 1983a, *ApJ* 274, 333
Rankin J.M., 1983b, *ApJ* 274, 359
Rankin J.M., 1990, *ApJ* 352, 247
Rankin J.M., 1993, *ApJ* 405, 285
Sieber W., 1997, *A&A* 321, 519
Sieradakis J.H., Gil J.A., Graham D.A. et al., 1995, *A&AS* 111, 205
Suleymanova S.A., Pugachev V.D., 1998, *AZh* 75, 287
Wu X., Manchester R.N., 1992, in: Hankins T.H., Rankin J.M., Gil J.A. (eds.), *Proc. of IAU Colloq. N128, The Magnetospheric Structure and Emission Mechanisms of Radio Pulsars*, Zielona Gora/ Poland: Pedagogical University Press, 362
Wu X., Xu W., Rankin J.M., 1992 in: Hankins T.H., Rankin J.M., Gil J.A. (eds.), *Proc. of IAU Colloq. N128, The Magnetospheric Structure and Emission Mechanisms of Radio Pulsars*, Zielona Gora/ Poland: Pedagogical University Press, 172
Wu X., Gao X., Rankin J.M., Xu W., Malofeev V.M., 1998, *AJ* 116, 1984